AIP | Chaos
An Interdisciplinary Journal of Nonlinear Science

The onset of chaos in orbital pilot-wave dynamics

Lucas D. Tambasco, Daniel M. Harris, Anand U. Oza, Rodolfo R. Rosales, and John W. M. Bush

Citation: Chaos **26**, 103107 (2016); doi: 10.1063/1.4964350
View online: http://dx.doi.org/10.1063/1.4964350
View Table of Contents: http://scitation.aip.org/content/aip/journal/chaos/26/10?ver=pdfcov
Published by the AIP Publishing

CHAOS **26**, 103107 (2016)

The onset of chaos in orbital pilot-wave dynamics

Lucas D. Tambasco,[1] Daniel M. Harris,[2] Anand U. Oza,[3] Rodolfo R. Rosales,[1] and John W. M. Bush[1,a)]
[1]Department of Mathematics, Massachusetts Institute of Technology, Cambridge, Massachusetts 02139, USA
[2]Department of Mathematics, University of North Carolina, Chapel Hill, North Carolina 27599, USA
[3]Courant Institute of Mathematical Sciences, New York University, New York, New York 10012, USA

(Received 15 June 2016; accepted 23 September 2016; published online 14 October 2016)

We present the results of a numerical investigation of the emergence of chaos in the orbital dynamics of droplets walking on a vertically vibrating fluid bath and acted upon by one of the three different external forces, specifically, Coriolis, Coulomb, or linear spring forces. As the vibrational forcing of the bath is increased progressively, circular orbits destabilize into wobbling orbits and eventually chaotic trajectories. We demonstrate that the route to chaos depends on the form of the external force. When acted upon by Coriolis or Coulomb forces, the droplet's orbital motion becomes chaotic through a period-doubling cascade. In the presence of a central harmonic potential, the transition to chaos follows a path reminiscent of the Ruelle-Takens-Newhouse scenario. *Published by AIP Publishing.* [http://dx.doi.org/10.1063/1.4964350]

A droplet may walk on the surface of a vertically vibrated fluid bath, propelled by the waves generated by its previous impacts. The resulting hydrodynamic pilot-wave system exhibits features that were once thought to be peculiar to quantum mechanics, such as tunneling, orbital quantization, and single-particle diffraction. Experimental evidence generally indicates that these quantum-like features become more pronounced as the forcing acceleration is increased, when the droplet is more strongly influenced by its wavefield. When subjected to external forces, walking droplets may execute stable circular orbits, provided the forcing acceleration is sufficiently low. As the forcing is progressively increased, these periodic orbits destabilize into wobbling orbits, then aperiodic and eventually chaotic trajectories. We here present the results of a theoretical exploration of this transition to chaos for three different pilot-wave systems, specifically droplets walking in the presence of Coriolis, linear spring, or Coulomb forces. Particular attention is given to detailing the manner in which stable circular orbits give way to chaotic motion as the forcing acceleration is increased. Our theoretical results are related to existing experiments whenever possible.

I. INTRODUCTION

A millimetric droplet can bounce in place indefinitely[1] on the surface of an oscillating fluid bath with vertical acceleration $\gamma \cos(2\pi f t)$. Provided $\gamma < \gamma_F$, where γ_F is the Faraday instability[2] threshold, the surface would remain flat in the absence of the drop. When the bouncing drop becomes synchronized with its wavefield, its bouncing period corresponds to the Faraday period $T_F = 2/f$, and it is said to be a resonant bouncer. Then, at each impact, it generates a localized field of Faraday waves with characteristic wavelength λ_F prescribed by the standard water-wave dispersion relation.[3] As the forcing amplitude is increased, the bouncing state destabilizes into a walking state [Fig. 1(a)], as was discovered a decade ago by Couder and collaborators.[4,5] These self-propelling droplets, henceforth "walkers," move in response to the wave field generated by their prior impacts and may exhibit behaviors reminiscent of quantum mechanical systems, such as tunneling,[6] single-particle diffraction,[7,8] and wave-like statistics in circular corrals.[9–11] This hydrodynamic pilot-wave system and its relation to realist models of quantum dynamics have been recently reviewed by Bush.[12,13]

Orbital pilot-wave dynamics were first examined by Fort *et al.*,[14] who demonstrated experimentally the quantization of orbital radii for walkers in a rotating frame [Fig. 1(b)], and rationalized this quantization with accompanying simulations. Owing to the identical forms of the Coriolis force acting on a mass moving in a rotating frame and the Lorentz force acting on a charge in a uniform magnetic field, the authors drew the analogy between these quantized inertial orbits and Landau levels in quantum mechanics. Harris and Bush[15] demonstrated experimentally that these quantized circular orbits can destabilize into wobbling and chaotic trajectories, features captured in the theoretical models of Oza

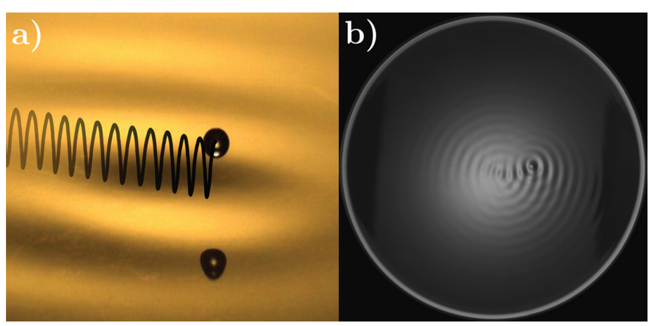

FIG. 1. (a) Oblique view of a resonant walker.[13] The solid line tracks the center of the walking droplet. (b) Top view of a walking droplet orbiting on a rotating bath,[15] a system to be explored numerically in Section III.

a)Electronic mail: bush@math.mit.edu

et al.[16,17] Perrard *et al.*[18] explored walkers in a harmonic potential and reported a double quantization of orbital radius and angular momentum, features also captured in their simulations.[19] In both of these orbital pilot-wave systems, the walker dynamics becomes complex and presumably chaotic for sufficiently high forcing acceleration γ. Nevertheless, traces of the unstable orbital solutions are evident in the emergent chaotic trajectories, which exhibit multimodal quantum-like statistics. The intriguing question raised by this hydrodynamic pilot-wave system is whether some form of chaotic pilot-wave dynamics might underlie the statistical behavior of microscopic particles, as described by standard quantum theory.[12,13]

Moláček and Bush[20,21] developed a theoretical description of the vertical and horizontal motion of the walking drops. Oza *et al.*[16] developed an integro-differential trajectory equation for the horizontal motion by considering that the vertical dynamics is fast relative to the horizontal dynamics. The resulting trajectory equation, henceforth referred to as the "stroboscopic model," is able to capture the supercritical pitchfork bifurcation from bouncing to walking, and the stability of straight-line walking along the direction of motion. Refined models of the wavefield have recently been developed by Milewski *et al.*,[22] Blanchette,[23] and Siéfert *et al.*[24] A reduced dynamical model for the horizontal dynamics of a constrained walker has been developed by Gilet[10] and examined by Rahman and Blackmore,[25] showing evidence of chaos.

Oza *et al.*[26] performed a linear stability analysis of orbital solutions to the stroboscopic trajectory equation in a rotating frame, predicting that all circular orbits are stable for sufficiently low forcing acceleration but that orbits of specific radii become unstable as the acceleration increases. A similar approach was followed by Labousse and Perrard[27] to examine orbital dynamics in a central harmonic potential. Oza *et al.*[17] numerically investigated the rich dynamical behavior of walkers in a rotating frame and concluded that for certain parameters the circular orbits may destabilize into wobbling, drifting, and eventually chaotic orbits, as seen experimentally.[15] We here detail the manner in which stable circular orbits, as arise in the presence of Coriolis, linear spring or Coulomb forces, give way to chaotic trajectories as the forcing acceleration is increased progressively.

In Section II, we review the stroboscopic model and numerical method used to simulate the drop's trajectories. We present the evolution from circular orbits to chaotic trajectories for drops subject to Coriolis (Section III), linear spring (Section IV), and Coulomb (Section V) forces. In Section VI, we discuss the two routes to chaos observed, specifically the classic period-doubling cascade for orbits in the presence of Coriolis and Coulomb forces, and a path to chaos reminiscent of the Ruelle-Takens-Newhouse scenario for orbital dynamics in the presence of a linear spring force.

II. TRAJECTORY EQUATION AND NUMERICAL METHOD

We first summarize the stroboscopic trajectory equation of Oza *et al.*[16] which forms the basis of our numerical investigation. We consider a resonant walker of mass m, bouncing with frequency $f/2$ on a vertically vibrated fluid bath shaken with forcing acceleration $\gamma\cos(2\pi ft)$ and subjected to an applied force $\boldsymbol{\mathcal{F}}$. We denote its horizontal position at time t by $\boldsymbol{x}_p(t) = (x_p(t), y_p(t))$. As shown by Moláček and Bush[21] and Oza *et al.*,[16] time-averaging the vertical dynamics leads to the integro-differential equation for the horizontal motion

$$m\ddot{\boldsymbol{x}}_p + D\dot{\boldsymbol{x}}_p = -mg\nabla h(\boldsymbol{x}_p(t), t) + \boldsymbol{\mathcal{F}}, \tag{1}$$

with the wavefield

$$h(\boldsymbol{x}, t) = \frac{A}{T_F}\int_{-\infty}^{t} J_0\left(k_F|\boldsymbol{x} - \boldsymbol{x}_p(s)|\right)\mathrm{e}^{-(t-s)/T_M}\,\mathrm{d}s,$$

where g is the gravitational acceleration, $T_F = 2/f$ is the Faraday period, and $k_F = 2\pi/\lambda_F$ is the wavenumber of the most unstable Faraday wave. We assume that the fluid bath consists of silicone oil with viscosity $\nu = 20$ cS, driven at $f = 80$ Hz, and that the walker has radius $R_D = 0.4$ mm and mass $m = 0.25$ mg. For this particular case, the time-averaged drag $D = 2.0$ mg/s and the wave amplitude $A = 3.5\,\mu$m were calculated from system parameters.[16,21] We note that A depends on the droplet's bouncing phase Φ, chosen such that $\sin\Phi = 0.2$ to provide the best fit between predicted and observed walking speeds.[16]

In addition to the applied force $\boldsymbol{\mathcal{F}}$, the walker experiences a drag force opposing its motion and a propulsive force proportional to the local slope of the interface. The wavefield h is expressed as the sum of waves generated by all prior droplet impacts. Contributions to the wavefield from previous impacts are exponentially damped over the memory timescale $T_M = T_d/(1 - \gamma/\gamma_F)$, where T_d is the wave decay time in the absence of forcing.[21,28] Note that the memory time is a monotonically increasing function of the forcing acceleration for $\gamma < \gamma_F$, so we will use the terms memory and vibrational forcing interchangeably in what follows.

We non-dimensionalize according to $\hat{\boldsymbol{x}} \to k_F\boldsymbol{x}$, $\hat{t} \to t/T_M$ and $\hat{\boldsymbol{\mathcal{F}}} \to k_F T_M \boldsymbol{\mathcal{F}}/D$. Dropping carets yields the dimensionless system

$$\begin{aligned}\kappa\ddot{\boldsymbol{x}}_p + \dot{\boldsymbol{x}}_p &= -\beta\nabla h(\boldsymbol{x}_p(t), t) + \boldsymbol{\mathcal{F}},\\ h(\boldsymbol{x}, t) &= \int_{-\infty}^{t} J_0(|\boldsymbol{x} - \boldsymbol{x}_p(s)|)\mathrm{e}^{-(t-s)}\,\mathrm{d}s,\end{aligned} \tag{2}$$

where $\kappa = m/DT_M$ and $\beta = mgAk_F^2T_M^2/DT_F$. This system is solved numerically by a fourth-order Adams-Bashforth linear multistep method, the details of which are reported elsewhere.[17] We initialize the simulations in a circular orbit, $\boldsymbol{x}_p(t) = r_0(\cos(\omega t), \sin(\omega t))$, where the orbital radius r_0 and angular frequency ω are solutions of the algebraic equations

$$\begin{aligned}-\kappa r_0\omega^2 &= \beta\int_0^\infty J_1\left(2r_0\sin\frac{\omega z}{2}\right)\sin\frac{\omega z}{2}\mathrm{e}^{-z}\,\mathrm{d}z + \boldsymbol{\mathcal{F}}\cdot\hat{\boldsymbol{r}},\\ r_0\omega &= \beta\int_0^\infty J_1\left(2r_0\sin\frac{\omega z}{2}\right)\cos\frac{\omega z}{2}\mathrm{e}^{-z}\,\mathrm{d}z + \boldsymbol{\mathcal{F}}\cdot\hat{\boldsymbol{\theta}},\end{aligned} \tag{3}$$

where $\hat{\boldsymbol{r}}$ and $\hat{\boldsymbol{\theta}}$ are the unit vectors in the radial and tangential directions, respectively. Eq. (3) guarantees that $\boldsymbol{x}_p(t) = r_0(\cos(\omega t), \sin(\omega t))$ is an exact solution of Eq. (2), which is stable for sufficiently low forcing acceleration γ/γ_F. After initializing the simulation in a stable circular orbit, we increase the forcing acceleration in increments of $\Delta(\gamma/\gamma_F)$, using the results from the previous simulation as the initial data. In order to resolve the bifurcations, we adapt the step value $\Delta(\gamma/\gamma_F)$, decreasing it as γ/γ_F increases. Each simulation is run using a dimensionless time step $\Delta t = 2^{-6}$ and up to a dimensionless time $t = 10^4$ in order to integrate beyond any transient behaviors.

III. CORIOLIS FORCE

We first consider the pilot-wave dynamics of a walking droplet in a frame rotating with angular frequency $\Omega = \Omega\hat{z}$. The walker experiences a Coriolis force, $\boldsymbol{\mathcal{F}} = -2m\Omega \times \dot{\boldsymbol{x}}_p$, which assumes the dimensionless form $\boldsymbol{\mathcal{F}} = -\hat{\Omega} \times \dot{\boldsymbol{x}}_p$, where $\hat{\Omega} = 2m\Omega/D$. It was demonstrated in prior experiments[14,15] that, in certain parameter regimes, the walkers execute circular orbits in the rotating frame of reference, $\boldsymbol{x}_p(t) = r_0(\cos\omega t, \sin\omega t)$. Above a critical value of the forcing acceleration, certain radii are forbidden; thus, the stable orbits are quantized in radius, roughly separated by half-integer multiples of the Faraday wavelength λ_F. The linear stability of the system, as elucidated by Oza *et al.*,[26] is summarized in Fig. 2. Laboratory experiments[15] and numerical simulations[17,29] revealed that, as the forcing acceleration is progressively increased, the quantized circular orbits destabilize into wobbling orbits, characterized by a periodic oscillation in the radius of curvature. As the memory is increased further, wobbling orbits then destabilize into drifting orbits,

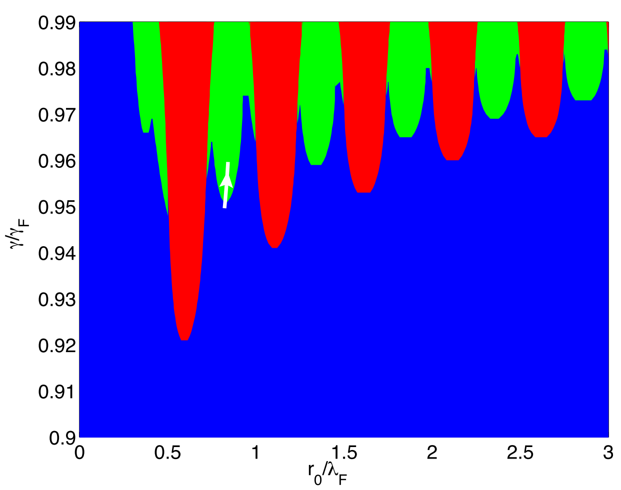

FIG. 2. Linear stability diagram[26] of orbital solutions of radius r_0 arising in the presence of a Coriolis force $\mathcal{F} = -2m\Omega \times \dot{\boldsymbol{x}}_p$. γ is the driving acceleration, γ_F is the Faraday threshold, and λ_F is the Faraday wavelength. The droplet's radius is $R_D = 0.4$ mm, impact phase $\sin\Phi = 0.2$, viscosity $\nu = 20$ cS, and forcing frequency 80 Hz. Blue regions indicate stable circular orbits. Green regions correspond to circular orbits that destabilize via an oscillatory instability. Red regions correspond to orbits that destabilize via a nonoscillatory instability. The transition to chaos is found by starting with an initially stable solution (r_0, ω, Ω) to Eq. (3) and increasing the dimensionless forcing acceleration γ/γ_F progressively while keeping Ω constant, following the procedure described in Section II. The white curve indicates the path through parameter space for the results shown in Section III. The transition to chaos through a period-doubling cascade appears to be generic in this system; specifically, it arises in passing from blue to green regions with increasing memory.

in which the orbital center drifts on a time scale that is long relative to the orbital period. Above a critical value of memory, the orbital dynamics becomes chaotic. We here characterize the progression from wobbling to drifting to chaotic dynamics as the memory is increased progressively.

Since the applied force is the Coriolis force, the circular orbits are not necessarily centered at the origin, so we cannot characterize the orbits simply by the radius $r(t) = |\boldsymbol{x}_p|$. We instead use the radius of curvature $R(t) = |\dot{\boldsymbol{x}}_p|^3/|\dot{\boldsymbol{x}}_p \times \ddot{\boldsymbol{x}}_p|$. Fig. 3 shows the trajectories obtained by numerically integrating Eq. (2) for a fixed dimensionless rotation rate $\hat{\Omega} = 0.6$ and progressively increasing memory. The resulting path through parameter space is indicated by the white curve in Fig. 2. In this parameter regime, the circular orbits have radius $r_0 \sim 0.8\lambda_F$ and period $T \sim 6T_M$. The linear stability analysis[26] of these orbits (see Fig. 2) indicates that they are stable for $\gamma/\gamma_F < 0.951$.

For $\gamma/\gamma_F \gtrsim 0.951$, the circular orbit destabilizes into a wobbling orbit with an oscillatory radius of curvature $R(t)$, as shown in Fig. 3(a). The frequency spectrum of $R(t)$ shows a single peak at the wobbling frequency $\omega_{\text{wobble}} \approx 2\omega$. As the memory is increased, the wobbling orbits destabilize into drifting orbits, where the radius of curvature $R(t)$ evidently undergoes a period-doubling bifurcation. These drifting orbits consist of roughly circular loops of radius $\mathcal{O}(r_0)$ and orbital period $T \approx 2\pi/\omega$ that slowly drift, such as those highlighted in red in the first column of Figs. 3(b)–3(e). Since the drifting is slow relative to T, we can define the orbital center for any loop

$$\boldsymbol{x}_c(t) \equiv \frac{1}{T}\int_t^{t+T} \boldsymbol{x}_p(s)\,\mathrm{d}s, \tag{4}$$

where T corresponds to the strongest peak in the power spectrum of $\boldsymbol{x}_p(t)$.

The orbital center for drifting orbits traces a circle on a timescale long relative to the orbital period ($t_{\text{drift}} \sim 100T$). Fig. 3(c) shows a period-4 drifting orbit at a still higher value of memory, which is confirmed by the presence of additional frequencies and their integer linear combinations in the frequency spectrum of $R(t)$. As the memory is increased progressively, the trajectories undergo a period-doubling cascade and eventually become chaotic, as suggested by the broadband frequency spectrum of $R(t)$ evident in Fig. 3(d). As one might expect, the trajectory of the orbital center $\boldsymbol{x}_c(t)$ is aperiodic for chaotic orbits.

Within the regime of chaotic trajectories, $\gamma/\gamma_F \geq 0.95994$, we observe a periodic window consisting of period-10 orbits, an example of which is shown in Fig. 3(e). The period-doubling cascade observed along the white path shown in Figure 2 is analogous to that seen in 1-dimensional unimodal maps. As the forcing acceleration is increased beyond the white curve, our system departs from the behavior of unimodal maps. In particular, we do not observe period-3 or period-5 windows for the parameters explored herein, but instead observe exotic orbits. An extensive numerical study of these exotic orbits in the case of a rotating frame is presented in Ref. 17.

The period-doubling cascade may be seen more clearly in the bifurcation diagram shown in Fig. 4. The points shown

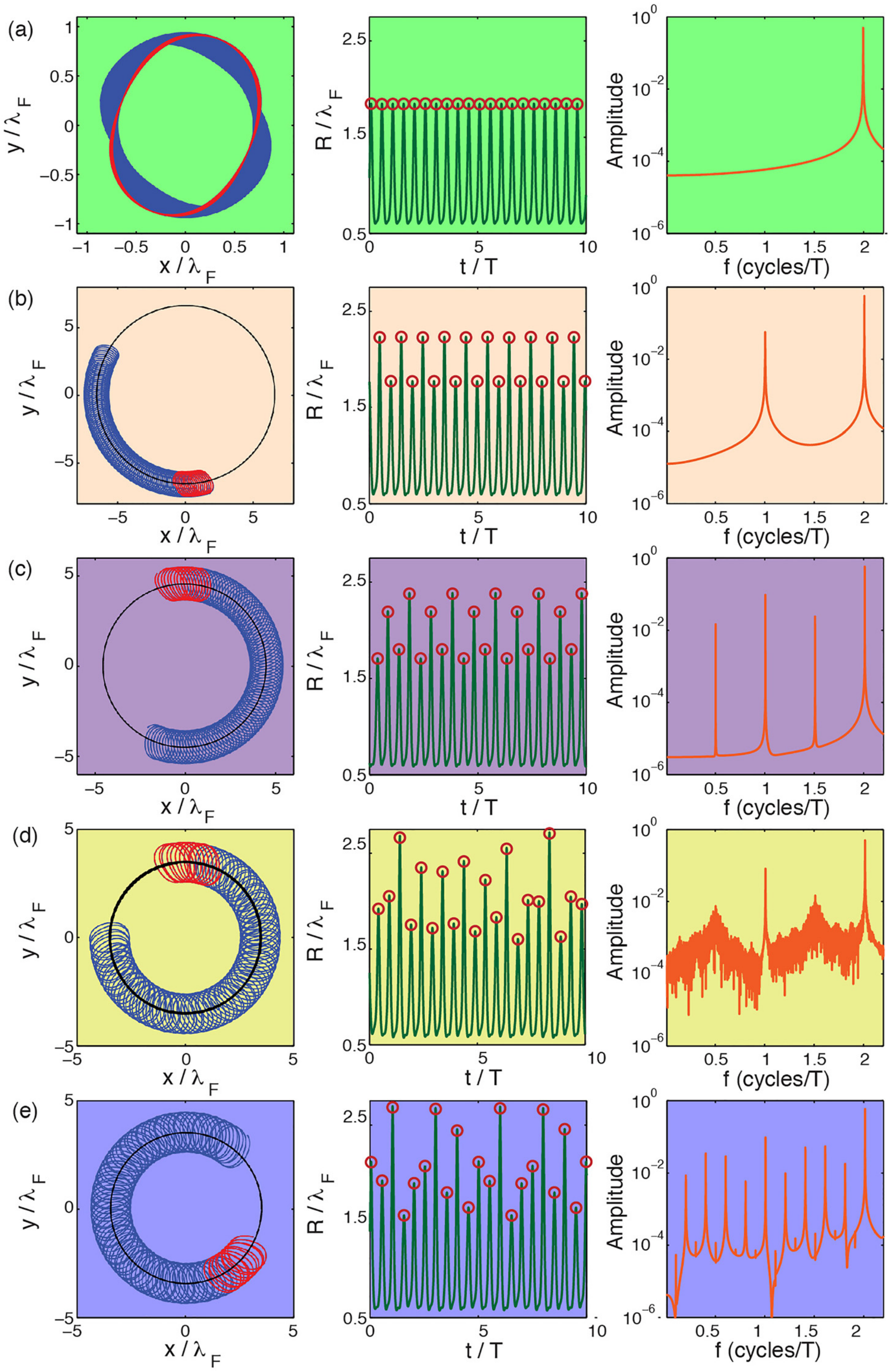

FIG. 3. Numerical solutions to the trajectory equation (Eq. (2)) with a Coriolis force $\mathcal{F} = -\hat{\Omega} \times \dot{\boldsymbol{x}}_p$, which describes pilot-wave dynamics in a rotating frame with dimensionless angular frequency $\hat{\Omega} = 0.6$. The first column shows the simulated trajectories $\boldsymbol{x}_p(t)$ plotted over 100 orbital periods T (blue), with the last 10 orbital periods (red) and the orbital center $\boldsymbol{x}_c(t)$ (black) superimposed. The second column shows the radius of curvature $R(t)$, with the local maxima greater than r_0 indicated by the red circles. The third column shows the frequency spectrum of $R(t)$. The rows correspond to (a) a wobbling orbit ($\gamma/\gamma_F = 0.957$), (b) a period-2 drifting orbit ($\gamma/\gamma_F = 0.959$), (c) a period-4 drifting orbit ($\gamma/\gamma_F = 0.9595$), (d) a chaotic trajectory ($\gamma/\gamma_F = 0.96004$), and (e) a period-10 orbit ($\gamma/\gamma_F = 0.960066$) in a periodic window within the chaotic regime.

correspond to local maxima $R_m > r_0$ in the radius of curvature $R(t)$, corresponding to the circles in the plots of $R(t)$ (middle column of Fig. 3). We note that the trajectory has secondary local maxima that are present throughout the period-doubling cascade and do not seem to affect it. Similar period-doubling cascades were observed for paths crossing from blue to green regions with increasing memory for other values of $\hat{\Omega}$ and larger values of the initial orbital radius r_0.

We now provide a qualitative explanation for why the period-doubling bifurcation coincides with the transition from wobbling to drifting orbits. Consider a simple model for a wobbling orbit, $\boldsymbol{x}_p(t) = r_0(1 + a_0 \cos \alpha\omega t)(\cos \omega t, \sin \omega t)$, where a_0 is the wobbling amplitude and $\alpha\omega$ is the wobbling frequency. Our linear stability analysis[26] has shown that circular orbits destabilize into wobbling orbits via a Hopf bifurcation as the memory is progressively increased and that the most unstable eigenvalues have imaginary part $\pm\alpha\omega$ with $\alpha \approx 2$. The linear theory only provides an estimate for the wobbling frequency near the onset of wobbling, but the numerical simulations in Fig. 3(a) confirm that the wobbling frequency is indeed approximately 2ω.

A simple model for a period-doubled orbit is thus given by

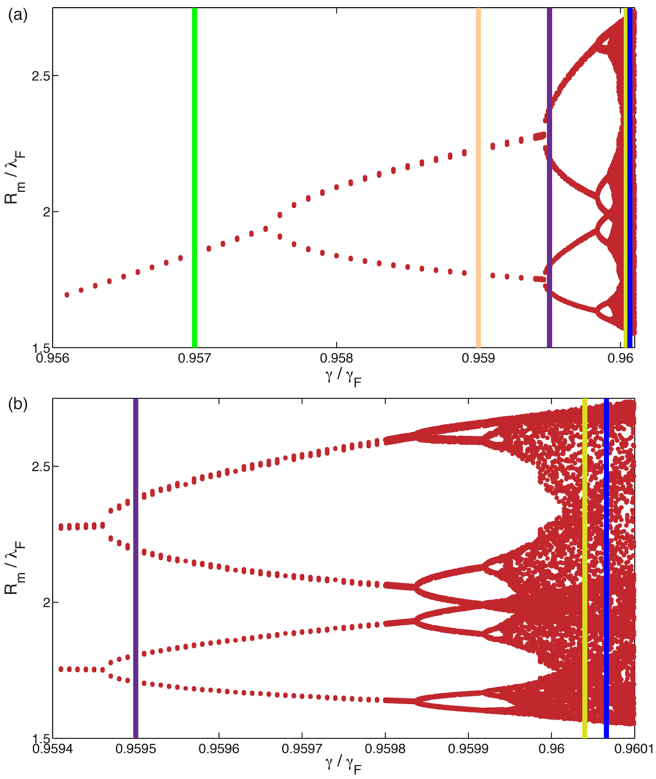

FIG. 4. Bifurcation diagrams showing the transition to chaos for a walker in a rotating frame with dimensionless angular frequency $\hat{\Omega} = 0.6$. For each value of the dimensionless forcing acceleration γ/γ_F, the points correspond to local maxima R_m in the radius of curvature $R(t)$. Panel (b) shows a magnified view illustrating the period-doubling cascade for $\gamma/\gamma_F > 0.9594$. The color-coded vertical lines correspond to the trajectories shown in Fig. 3. The dimensionless forcing acceleration is changed in increments of $\Delta(\gamma/\gamma_F) = 10^{-3}$ for $\gamma/\gamma_F \in [0.950, 0.956]$, $\Delta(\gamma/\gamma_F) = 10^{-4}$ for $\gamma/\gamma_F \in [0.9561, 0.9594]$, $\Delta(\gamma/\gamma_F) = 10^{-5}$ for $\gamma/\gamma_F \in [0.95941, 0.95980]$, and $\Delta(\gamma/\gamma_F) = 10^{-6}$ for $\gamma/\gamma_F \in [0.959801, 0.960099]$.

$$\boldsymbol{x}_p(t) = r_0[1 + a_0\cos(\alpha\omega t) + a_1\cos(\alpha\omega t/2)](\cos\omega t, \sin\omega t), \tag{5}$$

where a_0 is the wobbling amplitude and a_1 is the amplitude of the new period-doubled frequency. Note that, because α is close to 2, $\boldsymbol{x}_p(t)$ will consist of loops that do not close. Plugging the expression for $\boldsymbol{x}_p(t)$ into Eq. (4) yields an expression for the orbital center of the trajectory

$$\boldsymbol{x}_c(t) = \frac{r_0}{2}\sum_{i=0}^{1}\sum_{j=0}^{1} a_i \frac{\sin\pi\beta_{ij}}{\pi\beta_{ij}}\left(\cos\left[\beta_{ij}\Theta(t)\right], \sin\left[\beta_{ij}\Theta(t)\right]\right), \tag{6}$$

where $\Theta(t) = \omega t + \pi$ and $\beta_{ij} = \alpha/2^i + (-1)^j$. Because $\alpha \approx 2$, $\beta_{00} \approx 3$, $\beta_{10} \approx 2$, $\beta_{01} \approx 1$, and $\beta_{11} \approx 0$. Hence, the coefficients $\sin(\pi\beta_{ij})/\pi\beta_{ij}$ in Eq. (6) all nearly vanish, except for that corresponding to β_{11}, which leads to

$$\boldsymbol{x}_c(t) \approx -\frac{1}{2}a_1 r_0(\cos[\beta_{11}(\omega t + \pi)], \sin[\beta_{11}(\omega t + \pi)]). \tag{7}$$

This formula shows that the orbital center approximately traces out a circle of radius proportional to a_1 (the period-doubled amplitude), whose period $2\pi/(\beta_{11}\,\omega)$ is necessarily long relative to the orbital period T. In order for this argument to hold, the following conditions must be met.

Criterion 1: α must be close to but not exactly equal to 2.
Criterion 2: A period-doubling bifurcation must happen after the wobbling state emerges.

This argument provides a new rationale for the onset of period-doubling coinciding with the onset of drifting, a feature highlighted in previous experiments[15] and simulations.[17]

IV. SIMPLE HARMONIC POTENTIAL

We next consider the pilot-wave dynamics of a droplet walking in a harmonic potential. In this scenario, the walker is subjected to a radial spring force, $\boldsymbol{\mathcal{F}} = -k\boldsymbol{x}_p$. This system was realized experimentally by Perrard *et al.*[18,30] by encapsulating a small amount of ferromagnetic fluid in a walking droplet and exposing this compound droplet to a radially non-uniform vertical magnetic field. They demonstrated that, as the forcing amplitude is increased progressively, quantized circular orbits emerge, followed by more complex periodic and aperiodic trajectories. A key observation was the emergence of orbits that were quantized in both mean radius and angular momentum, a quantum-like feature also captured in their simulations. They also noted that in certain parameter regimes, an intermittent switching between the quantized periodic states could be observed.

We here confine our attention to the stability of the quantized circular orbits. As in Section III, we examine the transition from a stable circular orbit to a chaotic wobbling orbit as the forcing acceleration is increased. We proceed to demonstrate that the transition to chaos is qualitatively different. We characterize the orbits in terms of their local

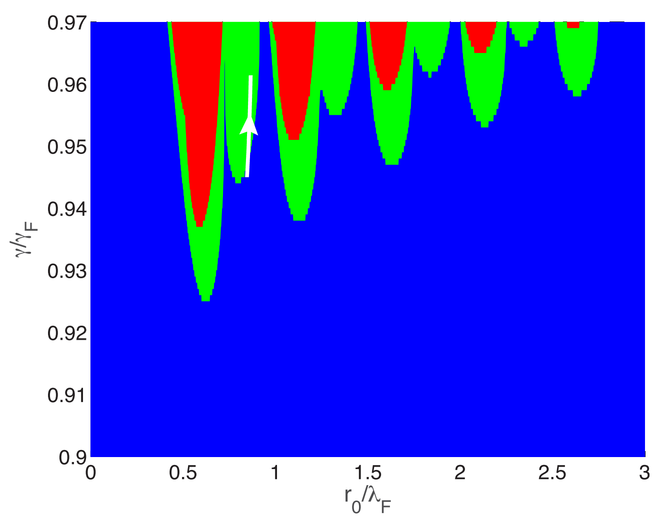

FIG. 5. Linear stability diagram[26] of orbital solutions of radius r_0 arising in the presence of a linear spring force $\boldsymbol{\mathcal{F}} = -k\boldsymbol{x}_p$. γ/γ_F is the dimensionless driving acceleration, and λ_F is the Faraday wavelength. The drop's radius is $R_D = 0.4$ mm, impact phase $\sin\Phi = 0.2$, viscosity $\nu = 20$ cS, and forcing frequency 80 Hz. Blue regions indicate stable circular orbits. Green regions correspond to circular orbits that destabilize via an oscillatory instability. Red regions correspond to orbits that destabilize via a nonoscillatory instability. The white curve indicates the path through parameter space for the results shown in Section IV. The transition to chaos is generic in this system; specifically, it arises in passing from blue to green regions with increasing memory.

radius $r(t) = |\boldsymbol{x}_p(t)|$, the distance to the center of the fixed harmonic potential, as well as the associated frequency spectrum.

The dimensional spring constant is here fixed to be $k = 3.2\,\mu$N/m which results in circular orbital solutions of radius $r_0 \sim 0.8\lambda_F$ for our choice of system parameters. For $\gamma/\gamma_F < 0.948$, these circular orbits are stable, in accordance with the linear stability analysis[19] summarized in Fig. 5. For $\gamma/\gamma_F \geq 0.948$, the circular orbit destabilizes into a wobbling orbit (Fig. 6(a)) whose radius oscillates with a single well-defined frequency f_1 that is approximately twice the orbital frequency $\omega/2\pi$. When the forcing acceleration is increased to $\gamma/\gamma_F = 0.9482$, a second independent frequency f_2 appears in the wobbling spectrum as shown in Fig. 6(b). Note that the additional peaks apparent in the spectrum of $r(t)$ correspond to integer linear combinations of the two base frequencies f_1 and f_2. As the forcing acceleration is increased further, the ratio of these frequencies changes continuously until they lock onto a fixed integer ratio at $\gamma/\gamma_F = 0.9495$ (Fig. 6(c)). For the simulations at higher memory, f_2 remains locked with f_1 in a ratio $f_2/f_1 = 1/4$. When the forcing acceleration reaches $\gamma/\gamma_F = 0.9610$, an additional incommensurate frequency f_3 (along with its integer linear combinations with f_1 and f_2) appears as shown in Fig. 6(d). Shortly after the appearance of this new frequency, for $\gamma/\gamma_F \geq 0.9613$, the spectrum begins to show evidence of broadband noise and the trajectory becomes chaotic, as shown in Fig. 6(e). Similar transitions to chaos were observed in other tongues for paths crossing from blue to green regions with increasing memory. We note that evidence of this particular route to chaos has also been observed in experiments.[31]

In summary, we observe a transition from a base state (circular orbit), to a single-frequency state (W1), to a

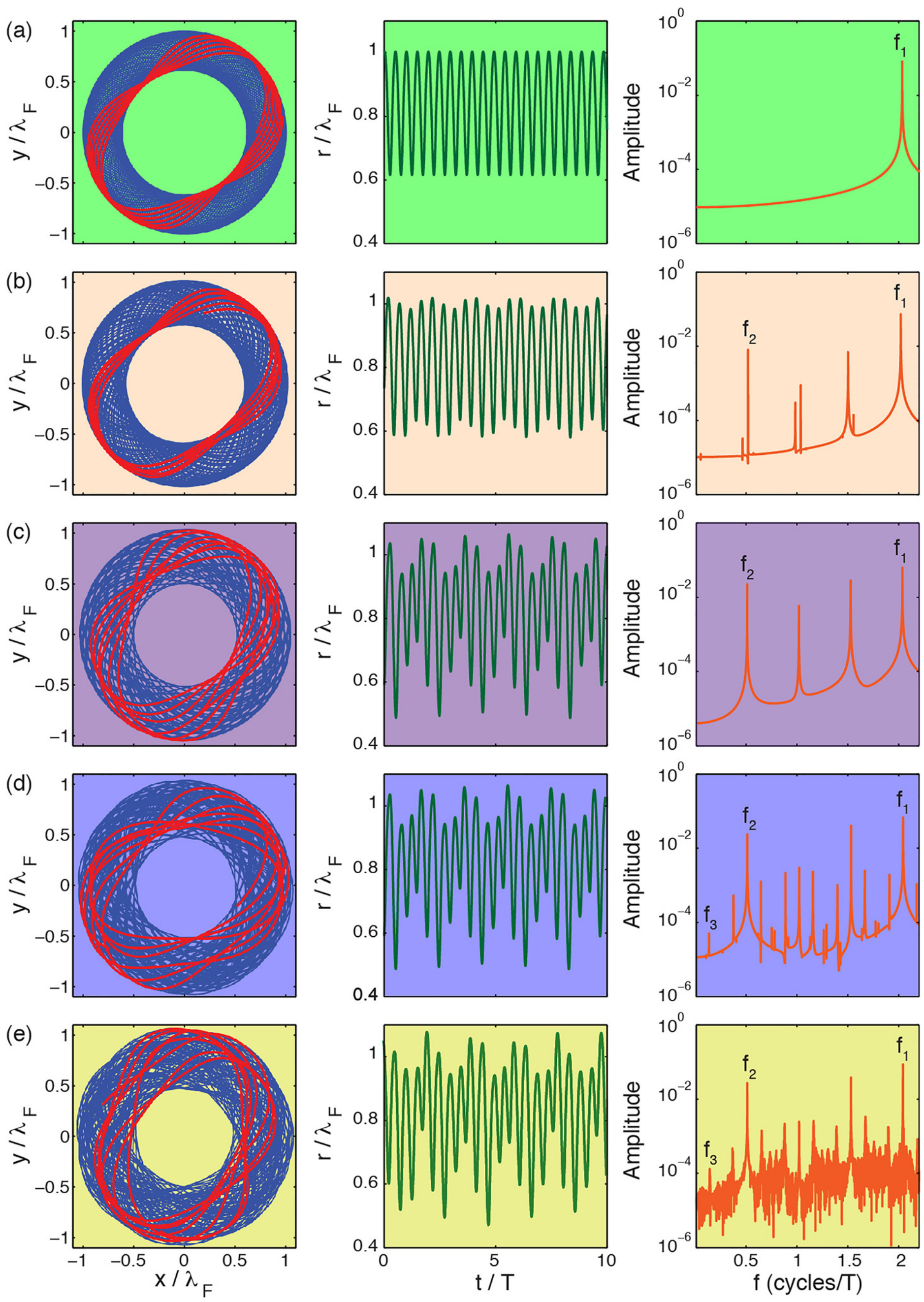

FIG. 6. Numerical solutions to the trajectory equation (Eq. (2)) with a spring force $\mathcal{F} = -k\boldsymbol{x}_p$ and a fixed dimensional spring constant $k = 3.2\,\mu$N/m which describes pilot-wave dynamics in a harmonic potential. The first column shows the simulated trajectories $\boldsymbol{x}_p(t)$ plotted over many orbital periods (blue) along with the last few orbital periods (red). The second column shows the orbital radius $r(t) = |\boldsymbol{x}_p(t)|$. The third column shows the frequency spectrum of $r(t)$. The rows correspond to (a) a wobbling orbit ($\gamma/\gamma_F = 0.9573$), (b) a quasiperiodic wobbling orbit ($\gamma/\gamma_F = 0.9583$), (c) a frequency-locked wobbling orbit ($\gamma/\gamma_F = 0.9600$), (d) a frequency-locked wobbling orbit with an additional incommensurate frequency ($\gamma/\gamma_F = 0.9610$), and (e) a chaotic trajectory ($\gamma/\gamma_F = 0.9613$).

two-frequency quasiperiodic state (W2), to a two-frequency frequency-locked state (W2*). Thereafter, a state with an additional incommensurate frequency emerges (W3), followed by a chaotic orbital state (C). This evolution can be summarized by the emergence of independent peaks in the frequency spectrum of $r(t)$ as shown in Fig. 7. This transition from a stable circular orbit to a chaotic wobbling orbit is notably different from the classic period-doubling transition but instead appears similar to the Ruelle-Takens-Newhouse route to chaos.[32,33] In the Ruelle-Takens-Newhouse scenario, a finite sequence of bifurcations gives rise to additional frequencies in the spectrum and after three such bifurcations, it is *likely* (but not guaranteed) that a strange attractor appears in phase space.[34]

V. 2D COULOMB POTENTIAL

Finally, we consider a walking droplet subject to a two-dimensional radial Coulomb force $\mathcal{F} = -Q\boldsymbol{x}_p/|\boldsymbol{x}_p|^2$. Such a force would correspond to a walking droplet with electric charge q attracted to an infinite line charge with charge density Λ placed at the origin normal to the fluid bath where $Q = q\Lambda/2\pi\epsilon_0$ (with electric constant $\epsilon_0 = 8.8 \times 10^{-12}$ F/m). In the dimensionless form, $\mathcal{F} = -\hat{Q}\boldsymbol{x}_p/|\boldsymbol{x}_p|^2$, where $\hat{Q} = Qk_F^2 T_M/D$. Although this system has yet to be realized experimentally, we can investigate it numerically using the integro-differential equation (2), which has been validated against experiments for walkers in Coriolis 15 and central harmonic[18] forces.

Note that circular orbits $\boldsymbol{x}_p(t) = r_0(\cos\omega t, \sin\omega t)$, with radius r_0 and orbital frequency ω, are exact solutions of Eq. (3) with an external Coulomb force $\mathcal{F}$. We assess linear stability of these solutions by a procedure analogous to that used by Oza *et al.*[26] and summarize our results in Fig. 8.

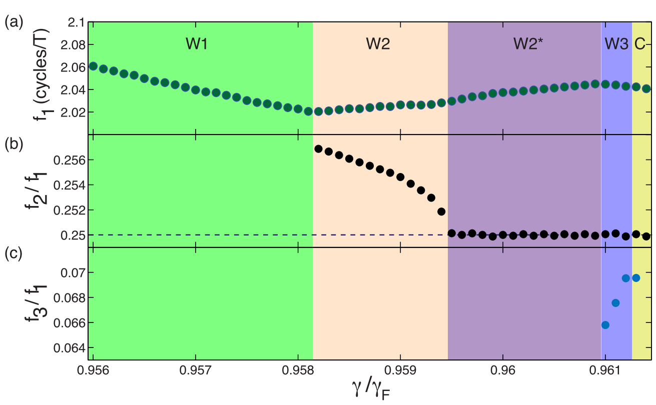

FIG. 7. Diagram detailing the evolution with memory of the independent peak frequencies in the spectrum of $r(t)$ arising during the transition to chaos in a harmonic potential with dimensional spring constant $k = 3.2\,\mu$N/m. Panel (a) tracks the principal wobbling frequency f_1, which first appears when the circular orbit becomes unstable. As the forcing acceleration is increased further, a second independent frequency f_2 appears, which later becomes locked with f_1 at $f_2/f_1 = 1/4$, as shown in panel (b). At higher accelerations, a third independent frequency f_3 appears that precedes the transition to a broadband spectrum in the chaotic regime, as shown in panel (c). We label W1 the single-frequency state, W2 the two-frequency quasiperiodic state, W2* the two-frequency frequency-locked state, W3 the state with a third incommensurate frequency, and C the chaotic orbital state. The dimensionless forcing acceleration is changed in increments of $\Delta(\gamma/\gamma_F) = 10^{-3}$ for $\gamma/\gamma_F \in [0.945, 0.956]$ and $\Delta(\gamma/\gamma_F) = 10^{-4}$ for $\gamma/\gamma_F \in [0.9560, 0.9614]$.

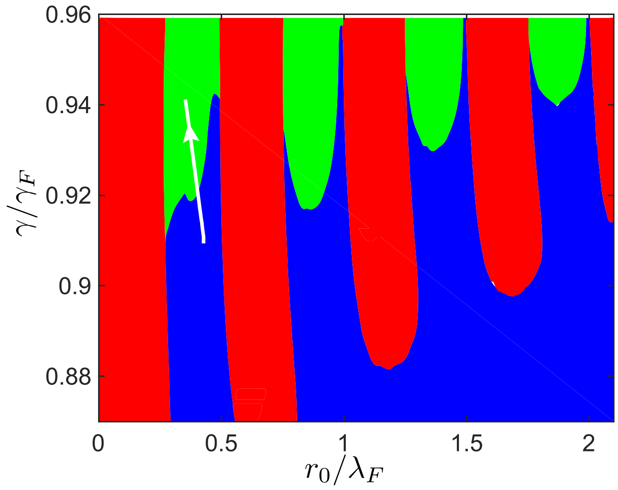

FIG. 8. Linear stability diagram of orbital solutions of radius r_0 arising in the presence of a 2D Coulomb force $\mathcal{F} = -Q\boldsymbol{x}_p/|\boldsymbol{x}_p|^2$. γ/γ_F is the dimensionless driving acceleration and λ_F is the Faraday wavelength. Blue regions indicate stable circular orbits. Green regions correspond to circular orbits that destabilize via an oscillatory instability. Red regions correspond to orbits that destabilize via a nonoscillatory instability. The transition to chaos is tracked along the white curve by finding an initial stable solution (r_0, ω, Q) to Eq. (3) and increasing the dimensionless forcing acceleration γ/γ_F progressively while keeping Q constant.

Orbits with radii $0.3 < r_0/\lambda_F < 0.5$ are predicted to be stable provided $\gamma/\gamma_F < 0.915$. Thus, we initialize the simulation with $\gamma/\gamma_F = 0.91$ and a fixed charge parameter $Q = 0.35$ nJ that corresponds to a stable circular orbit of radius $r_0 = 0.385\lambda_F$. We evolve the system as described in Section II with an initial increment of $\Delta(\gamma/\gamma_F) = 10^{-3}$.

As indicated by the linear stability analysis (Fig. 8), the circular orbit becomes unstable to a wobbling orbit at $\gamma/\gamma_F \gtrsim 0.920$. An example of a wobbling orbit is shown in the first panel of Fig. 9(a) for $\gamma/\gamma_F = 0.9375$. We use the fact that the system has an imposed center to characterize the trajectory by its radius $r(t) = |\boldsymbol{x}_p(t)|$, plotted in the second panel of Fig. 9(a), which exhibits a periodic oscillation between two values. The frequency spectrum of $r(t)$, shown in the third panel of Fig. 9(a), indicates that the wobbling frequency is $\omega_{\text{wobble}} \sim 0.65\omega$. Since $\omega_{\text{wobble}}/\omega$ is not close to 2 (criterion 1), this system does not exhibit drifting orbits.

As the memory is further increased, the frequency spectra shown in the last column of Fig. 9 exhibit evidence of successive period-doubling bifurcations: half-frequencies $\omega_{\text{wobble}}/2$ emerge at $\gamma/\gamma_F \sim 0.9394$, quarter-frequencies at $\gamma/\gamma_F \sim 0.94141$, and eventually a broadband frequency spectrum at $\gamma/\gamma_F \sim 0.941791$, evidence of chaotic dynamics. We also see a period-20 orbit when $\gamma/\gamma_F \sim 0.941815$ (Fig. 9(e)), an example of a periodic window within the chaotic regime. The period-doubling cascade is more clearly evident in Fig. 10, where we plot the local maxima r_m of the radius $r(t)$ as a function of the forcing acceleration γ/γ_F.

Unlike those arising in the presence of a Coriolis force or a simple harmonic potential, the transition to chaos was specific to the leftmost green tongue (Fig. 8), where it was observed for different initial radii $0.3 < r_0/\lambda_F < 0.5$ and corresponding Q. Chaotic orbits have not been observed in other isolated regions of oscillatory instability, where

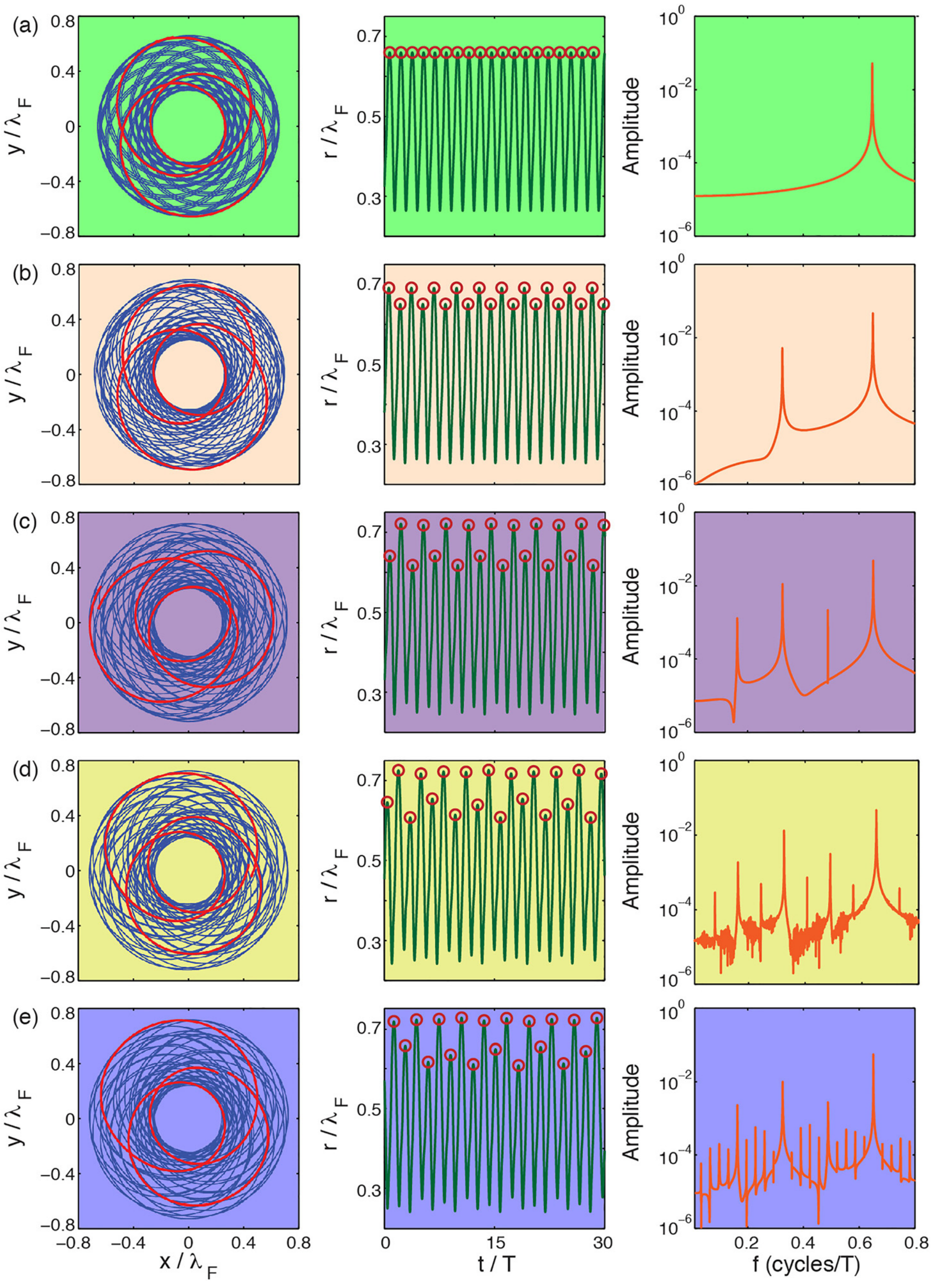

FIG. 9. Numerical simulations of Eq. (2) with $\mathcal{F} = -Q\boldsymbol{x}_p/|\boldsymbol{x}_p|^2$, which describes the pilot-wave dynamics of a walking droplet subject to a two-dimensional Coulomb force. The first column shows the trajectory $\boldsymbol{x}_p(t) = (x_p(t), y_p(t))$ with the long term trajectory shown in blue, and the last few orbits colored red. The radius of the orbit $r(t) = |\boldsymbol{x}_p(t)|$ is plotted in the middle column with local maxima r_m indicated by red circles. The third column shows the frequency spectrum of $r(t)$. The memory parameter is progressively increased from panels (a) through (e) with rows corresponding to: (a) a wobbling orbit ($\gamma/\gamma_F = 0.9375$), (b) a period-2 wobbling orbit ($\gamma/\gamma_F = 0.9394$), (c) a period-4 wobbling orbit ($\gamma/\gamma_F = 0.94141$), (d) a chaotic trajectory ($\gamma/\gamma_F = 0.941791$), and (e) a period-20 orbit ($\gamma/\gamma_F = 0.941815$) in a periodic window within the chaotic regime.

unstable orbits tend to spiral into the center or away to infinity instead of undergoing a period-doubling cascade.

VI. CONCLUSIONS

We have characterized the transition from stable circular orbits to chaos in three pilot-wave systems as the forcing acceleration is increased progressively. Walking droplets subject to Coriolis (Section III) and Coulomb (Section V) forces follow a period-doubling route to chaos, whereby circular orbits are destabilized into wobbling trajectories of increasing complexity. The main difference between these two scenarios, arising from the fact that the rotating system does not have a fixed center of force, is the existence of drifting orbits in the rotating frame. These orbits emerge when a wobbling orbit of frequency approximately twice the orbital frequency undergoes a period-doubling bifurcation. The rotating system is thus seen to support stable nonlinear states characterized by a drifting self-orbiting motion, which are related to the hydrodynamic spin states discussed in Refs. 12, 26, and 35.

The case of a walking droplet in a simple harmonic potential (Section IV) exhibits an entirely different transition to chaos. The circular orbits destabilize into wobbling orbits, but successive bifurcations lead to the appearance of new independent frequencies in the power spectrum of the orbital radius. These independent frequencies eventually lock; subsequently, just before the chaotic regime, we see the emergence of an additional incommensurate frequency. The observed transition is similar to the Ruelle-Takens-Newhouse route to chaos, as has been observed previously in other fluid systems, including Rayleigh-Bernard convection[36] and Taylor-Couette flow,[37] as well as in simulations of converging-diverging channel flows.[38]

As noted in the experimental realizations of walking droplets subject to Coriolis[15] and central[18] forces, increasing

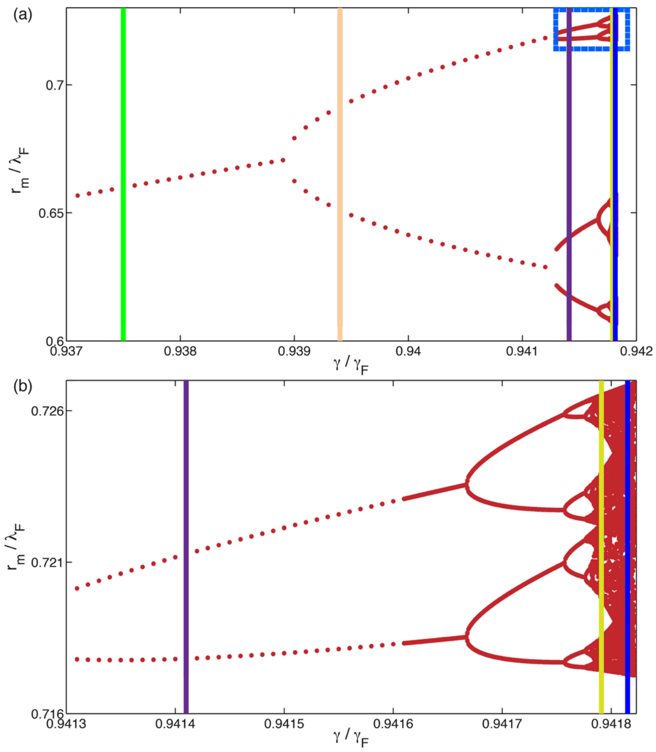

FIG. 10. Bifurcation diagrams showing the route to chaos for a walking droplet subject to a two-dimensional Coulomb force with charge parameter $Q = 0.35$ nJ. We track the local maxima r_m of the orbital radius $r(t) = |\boldsymbol{x}_p|$ as a function of the non-dimensional forcing acceleration γ/γ_F. Panel (b) gives a magnified view of the upper right corner (delineated by the blue box) of panel (a), showing the details of the period-doubling cascade immediately preceding the transition to chaos. Color-coded vertical lines correspond to the trajectories depicted in Fig. 9. The dimensionless forcing acceleration is changed in increments of $\Delta(\gamma/\gamma_F) = 10^{-3}$ for $\gamma/\gamma_F \in [0.910, 0.936]$, $\Delta(\gamma/\gamma_F) = 10^{-4}$ for $\gamma/\gamma_F \in [0.9361, 0.9413]$, $\Delta(\gamma/\gamma_F) = 10^{-5}$ for $\gamma/\gamma_F \in [0.94131, 0.94161]$, and $\Delta(\gamma/\gamma_F) = 10^{-6}$ for $\gamma/\gamma_F \in [0.941611, 0.941900]$.

the forcing acceleration has the effect of destabilizing circular orbits. The evolution from stable circular orbits to chaotic trajectories occurs over a small range $\Delta(\gamma/\gamma_F) \sim 10^{-4}$; thus, resolving this transition requires extremely precise experiments. In our numerical investigation, we were able to capture the details of each bifurcation and explore the transition to chaos by finely adjusting our memory parameter. For Coulomb and Coriolis forces, we note that the forcing acceleration was increased by increments as small as $\Delta(\gamma/\gamma_F) = 10^{-6}$, which allowed us to capture period-16 and period-32 orbits within exceedingly narrow parameter windows. Such an exploration is not possible with current experimental capabilities.[39]

Relating the periodic and quasiperiodic trajectories observed at low memory to the multimodal statistical behavior of chaotic trajectories in the high-memory limit is the subject of ongoing research. Establishing a quantitative link between the unstable periodic orbits and the emergent statistical behavior in the high-memory limit is an objective reminiscent of that of Gutzwiller, who related classical periodic orbits with solutions of the time-independent Schrödinger equation.[40] It is hoped that this paper, the first theoretical investigation of routes to chaos in a pilot-wave system, will attract the attention of the dynamical systems community to a remarkably rich new class of problems.

ACKNOWLEDGMENTS

J.B. gratefully acknowledges the financial support of the NSF through Grant No. CMMI-1333242. The work of R.R. was partially supported by NSF Grant No. DMS-1318942. A.O. acknowledges the support of the NSF Mathematical Sciences Postdoctoral Research Fellowship. The authors acknowledge the support of MIT-Brazil. We thank L. Faria and S. Perrard for valuable discussions.

[1] J. Walker, “Drops of liquid can be made to float on the liquid. What enables them to do so?,” Sci. Am. **238**(6), 151–158 (1978).
[2] T. B. Benjamin and F. Ursell, “The stability of the plane free surface of a liquid in vertical periodic motion,” Proc. R. Soc. A **225**, 505–515 (1954).
[3] K. Kumar, “Linear theory of Faraday instability in viscous fluids,” Proc. R. Soc. A **452**, 1113–1126 (1996).
[4] Y. Couder, S. Protière, E. Fort, and A. Boudaoud, “Dynamical phenomena: Walking and orbiting droplets,” Nature **437**, 208 (2005).
[5] S. Protière, A. Boudaoud, and Y. Couder, “Particle-wave association on a fluid interface,” J. Fluid Mech. **554**, 85–108 (2006).
[6] A. Eddi, E. Fort, F. Moisy, and Y. Couder, “Unpredictable tunneling of a classical wave-particle association,” Phys. Rev. Lett. **102**, 240401 (2009).
[7] Y. Couder and E. Fort, “Single-particle diffraction and interference at a macroscopic scale,” Phys. Rev. Lett. **97**, 154101 (2006).
[8] A. Andersen, J. Madsen, C. Reichelt, S. Ahl, B. Lautrup, C. Ellegaard, M. Levinsen, and T. Bohr, “Double-slit experiment with single wave-driven particles and its relation to quantum mechanics,” Phys. Rev. E **92**, 14 (2015).
[9] D. M. Harris, J. Moukhtar, E. Fort, Y. Couder, and J. W. M. Bush, “Wavelike statistics from pilot-wave dynamics in a circular corral,” Phys. Rev. E **88**, 011001 (2013).
[10] T. Gilet, “Dynamics and statistics of wave-particle interactions in a confined geometry,” Phys. Rev. E **90**, 052917 (2014).
[11] T. Gilet, “Quantumlike statistics of deterministic wave-particle interactions in a circular cavity,” Phys. Rev. E **93**, 042202 (2016).
[12] J. W. M. Bush, “Pilot-wave hydrodynamics,” Annu. Rev. Fluid Mech. **47**, 269–292 (2015).
[13] J. W. M. Bush, “The new wave of pilot-wave theory,” Phys. Today **68**(8), 47 (2015).
[14] E. Fort, A. Eddi, A. Boudaoud, J. Moukhtar, and Y. Couder, “Path-memory induced quantization of classical orbits,” Proc. Natl. Acad. Sci. U.S.A. **107**, 17515–17520 (2010).
[15] D. M. Harris and J. W. M. Bush, “Droplets walking in a rotating frame: From quantized orbits to multimodal statistics,” J. Fluid Mech. **739**, 444–464 (2014).
[16] A. U. Oza, R. R. Rosales, and J. W. M. Bush, “A trajectory equation for walking droplets: Hydrodynamic pilot-wave theory,” J. Fluid Mech. **737**, 552–570 (2013).
[17] A. U. Oza, Ø. Wind-Willassen, D. M. Harris, R. R. Rosales, and J. W. M. Bush, “Pilot-wave hydrodynamics in a rotating frame: Exotic orbits,” Phys. Fluids **26**, 082101 (2014).
[18] S. Perrard, M. Labousse, M. Miskin, E. Fort, and Y. Couder, “Self-organization into quantized eigenstates of a classical wave-driven particle,” Nat. Commun. **5**, 3219 (2014).
[19] M. Labousse, A. U. Oza, S. Perrard, and J. W. M. Bush, “Pilot-wave dynamics in a harmonic potential: Quantization and stability of circular orbits,” Phys. Rev. E **93**, 033122 (2016).
[20] J. Moláček and J. W. M. Bush, “Drops bouncing on a vibrating bath,” J. Fluid Mech. **727**, 582–611 (2013).
[21] J. Moláček and J. W. M. Bush, “Drops walking on a vibrating bath: Towards a hydrodynamic pilot-wave theory,” J. Fluid Mech. **727**, 612–647 (2013).
[22] P. Milewski, C. Galeano-Rios, A. Nachbin, and J. W. M. Bush, “Faraday pilot-wave dynamics: Modelling and computation,” J. Fluid Mech. **778**, 361–388 (2015).
[23] F. Blanchette, “Modeling the vertical motion of drops bouncing on a bounded fluid reservoir,” Phys. Fluids **28**, 032104 (2016).
[24] A. U. Oza, E. Siéfert, D. M. Harris, J. Moláček, and J. W. M. Bush, “Orbiting pairs of walking droplets,” (submitted).
[25] A. Rahman and D. Blackmore, “Neimark-Sacker bifurcations and evidence of chaos in a discrete dynamical model of walkers,” Chaos, Solitons Fractals **91**, 339–349 (2016).
[26] A. U. Oza, D. M. Harris, R. R. Rosales, and J. W. M. Bush, “Pilot-wave dynamics in a rotating frame: On the emergence of orbital quantization,” J. Fluid Mech. **744**, 404–429 (2014).

[27]M. Labousse and S. Perrard, "Non-Hamiltonian features of a classical pilot-wave dynamics," Phys. Rev. E **90**, 022913 (2014).
[28]A. Eddi, E. Sultan, J. Moukhtar, E. Fort, M. Rossi, and Y. Couder, "Information stored in Faraday waves: The origin of path memory," J. Fluid Mech. **675**, 433–463 (2011).
[29]D. M. Harris, "The pilot-wave dynamics of walking droplets in confinement," Ph.D. thesis, Massachusetts Institute of Technology, Department of Mathematics, 2015.
[30]S. Perrard, M. Labousse, E. Fort, and Y. Couder, "Chaos driven by interfering memory," Phys. Rev. Lett. **113**, 104101 (2014).
[31]S. Perrard, "A wave-mediated memory: Eigenstates, chaos and probabilities," Ph.D. thesis, Université Paris Diderot, 2014.
[32]D. Ruelle and F. Takens, "On the nature of turbulence," Commun. Math. Phys. **20**, 167–192 (1971).
[33]S. Newhouse, D. Ruelle, and F. Takens, "Occurrence of strange axiom A attractors near quasi periodic flows on T^m, $m \geq 3$," Commun. Math. Phys. **64**, 35–40 (1978).
[34]J.-P. Eckmann, "Roads to turbulence in dissipative dynamical systems," Rev. Mod. Phys. **53**, 643 (1981).
[35]M. Labousse, "Etude d'une dynamique à mémoire de chemin: une expérimentation théorique," Ph.D. thesis, Université Pierre et Marie Curie-Paris VI, 2014.
[36]J. Gollub and S. Benson, "Many routes to turbulent convection," J. Fluid Mech. **100**, 449–470 (1980).
[37]J. P. Gollub and H. L. Swinney, "Onset of turbulence in a rotating fluid," Phys. Rev. Lett. **35**, 927 (1975).
[38]A. Guzmán and C. Amon, "Transition to chaos in converging–diverging channel flows: Ruelle–Takens–Newhouse scenario," Phys. Fluids **6**, 1994–2002 (1994).
[39]D. M. Harris and J. W. Bush, "Generating uniaxial vibration with an electrodynamic shaker and external air bearing," J. Sound Vib. **334**, 255–269 (2015).
[40]M. C. Gutzwiller, "Periodic orbits and classical quantization conditions," J. Math. Phys. **12**, 343–358 (1971).